UDC 621.313 https://doi.org/10.20998/2074-272X.2026.4.05

Q.T. Nguyen, C.D. Tran

An enhanced sliding mode observer method applied to sensorless induction motor drives under stator resistance variation

Introduction. *Sliding mode observer (SMO), with its simplicity and efficiency, is one of the widely used sensorless control techniques in induction motor (IM) drive systems. However, this method's performance is highly sensitive to changes in motor parameters, especially increases in stator resistance (R_s) due to thermal effects.* ***Problem.*** *As R_s increases due to thermal effects during operation, the estimation of rotor flux and virtual current becomes inaccurate, degrading the SMO method's performance in generating estimated speeds for the controller.* ***Goal.*** *To develop an improved speed sensorless control scheme for IM drives that maintains high accuracy of estimation under variations in R_s.* ***Methodology.*** *SMO is first employed to estimate rotor speed from measured stator currents and voltages. Then, a R_s estimation mechanism based on a combined SMO-model reference adaptive system (SMO-MRAS) structure is proposed, in which the voltage model serves as the reference model and the SMO-based flux estimation acts as the adaptive model. The estimated resistance is obtained through a PI adaptation law.* ***Results.*** *Under 20 % and 40 % R_s increments, the proposed scheme reduces Integral Absolute Error (IAE) from 0.7699 to 0.4661, Integral Squared Error (ISE) from 0.555 to 0.4688, and Integral Time Squared Error (ITSE) from 0.6286 to 0.4502. The maximum stator current deviation decreases from 0.578 A to 0.005457 A, while stable speed tracking at 20 rad/s is preserved under load disturbance.* ***Scientific novelty.*** *The study proposes a structurally integrated SMO-MRAS framework that decouples speed estimation from MRAS while embedding resistance adaptation within the observer loop.* ***Practical value.*** *The proposed method enhances robustness against thermal parameter variation and improves the reliability of sensorless IM drives in real operating conditions.* References 36, table 1, figures 9.

Key words: **resistance variation, speed sensorless control, sliding mode observer, thermal effect, voltage model.**

Вступ. *Спостерігач ковзного режиму (SMO) завдяки своїй простоті та ефективності є одним із найбільш поширених методів бездатчикового керування в системах електропривода на базі асинхронних двигунів (ІМ). Проте ефективність цього методу значною мірою залежить від зміни параметрів двигуна, особливо від збільшення опору статора R_s, спричиненого тепловими ефектами.* ***Проблема***. *Зі збільшенням R_s у процесі роботи внаслідок нагрівання погіршується точність оцінювання потокозчеплення ротора та віртуального струму, що негативно впливає на якість формування оціненої швидкості для системи керування на основі SMO.* ***Мета***. *Розроблення вдосконаленої системи бездатчикового керування швидкістю приводів для ІМ, здатної забезпечувати високу точність оцінювання за умов зміни опору статора R_s.* ***Методика***. *На першому етапі SMO використовується для оцінювання швидкості ротора за виміряними струмами та напругами статора. Далі запропоновано механізм оцінювання R_s на базі комбінованої структури адаптивної системи на основі моделі SMO (SMO-MRAS), у якій модель напруги використовується як еталонна модель, а оцінювання потоку на основі SMO – як адаптивна модель. Оцінювання опору здійснюється за допомогою PI-закону адаптації.* ***Результати***. *При збільшенні R_s на 20 % і 40 % запропонована схема забезпечує зменшення інтеграла абсолютної похибки (IAE) з 0,7699 до 0,4661, інтеграла квадрата похибки (ISE) з 0,555 до 0,4688 та інтеграла квадрата похибки, зваженого за часом (ITSE), з 0,6286 до 0,4502. Максимальне відхилення струму статора зменшується з 0,578 А до 0,005457 А, при цьому забезпечується стабільне відстеження швидкості на рівні 20 рад/с за наявності збурення навантаження.* ***Наукова новизна***. *Запропоновано структурно інтегровану схему SMO-MRAS, у якій процес оцінювання швидкості відокремлений від MRAS, а механізм адаптації опору інтегрований безпосередньо в контур спостерігача.* ***Практична значимість***. *Запропонований метод підвищує робастність системи до теплових змін параметрів та покращує надійність бездатчикових асинхронних електроприводів у реальних умовах експлуатації.*. Бібл. 36, табл. 1, рис. 9.

Ключові слова: **зміна опору, безсенсорне керування швидкістю, спостерігач ковзного режиму, тепловий ефект, модель напруги.**

Introduction. High-performance induction motor (IM) drives continue to play a key role in industrial, transportation, and renewable-energy applications due to their robustness, cost-effectiveness, and favorable power density. Nevertheless, achieving accurate speed and torque regulation remains challenging, particularly under load disturbances and parameter variations. Among existing strategies, field-oriented control (FOC) is widely employed thanks to its ability to decouple torque and flux dynamics, enabling fast transient response and high steady-state accuracy [1–5]. However, the effectiveness of typical FOC strongly depends on model accuracy; in particular, variations in R_s due to thermal effects significantly degrade flux and angle reconstruction, especially at low speeds [6].

Alongside FOC, direct torque control (DTC) has attracted considerable attention because of its simple structure and rapid torque response. Recent studies focus on improving voltage vector selection and reducing torque ripple and harmonics through advanced or intelligent techniques [7–10]. Despite these efforts, DTC still faces inherent trade-offs among torque ripple, switching frequency, and robustness over a wide speed range. In contrast, scalar control remains attractive in low-cost applications owing to its simplicity and minimal sensing requirements, although its dynamic performance and low-speed behavior are inherently limited. To address these drawbacks, adaptive and closed-loop scalar schemes have been proposed to enhance starting torque and regulation capability [11, 12]. Beyond nominal operation, the reliability of IM drives increasingly relies on fault-tolerant strategies; observer-based sensor fault diagnosis and reconfiguration within FOC frameworks have demonstrated the ability to maintain stable operation when current or speed measurements become unreliable [13].

These considerations highlight two closely related practical requirements in modern IM drive systems. On the one hand, speed-sensorless control has become increasingly important for reducing system cost and wiring complexity while enhancing reliability and fault tolerance in demanding operating environments. On the other hand, variations in the R_s directly and detrimentally affect flux estimation accuracy, which propagates through the control loop and degrades overall performance. Consequently, estimating and compensating for R_s are essential to ensure reliable operation, particularly at low speeds and during thermal transients. These challenges provide strong motivation for a critical review of recent developments in sensorless control and parameter estimation, intending to identify unresolved issues and research opportunities.

© Q.T. Nguyen, C.D. Tran

Review of recent publications and selection of unsolved tasks. Recent studies on sensorless IM drives can be broadly classified according to the adopted estimation principle and robustness strategy. Neural network approaches aim to reduce model dependency through data-driven mappings. Dual-field-oriented sensorless schemes have been proposed to alleviate parameter sensitivity [14], while neural observers have been combined with robust control techniques to address disturbances and voltage saturation, primarily demonstrated on permanent magnet synchronous motors (PMSMs) [15]. Artificial neural network (ANN)-based sensorless estimation has also been reported for brushless DC drives [16]. Despite their potential, these methods often suffer from limited generalization under thermal parameter variations.

Kalman filter (KF) estimators remain attractive due to their stochastic framework and noise-handling capability. Extended KF-assisted sensorless IM control has been combined with advanced control structures, including fractional-order controllers [17], and integrated into sensorless predictive control schemes with experimental validation [18]. Comparative studies and Unscented KF-based solutions have also been reported for PMSM drives [19, 20]. However, their practical application is constrained by computational complexity, sensitivity to noise covariance tuning, and degraded performance under model mismatch, particularly at low speeds.

Within the model reference adaptive system (MRAS) family, current-based MRAS has been extensively investigated, with stability enhancement techniques and sensitivity analyses addressing known instability regions and parameter dependence [21, 22]. Alternative MRAS formulations include reactive-power MRAS, sometimes augmented with neural components to extend the operating range [23], and stator-flux-based MRAS schemes, which further emphasize the importance of flux estimation accuracy in sensorless control [24]. In rotor-flux-based MRAS, rotor flux angle estimation remains central to sensorless FOC applications [25, 26].

Finally, sliding mode observer (SMO) approaches emphasize robustness to uncertainties. A fractional-order super-twisting SMO with flux linkage compensation targets the chattering and accuracy trade-off [27]; SMO has also been tailored to speed-sensorless linear IM drives [28], and combined neural/fractional sliding-mode schemes have been explored for bearingless IM [29]. Furthermore, the proven robustness of sliding mode principles in advanced sliding mode control frameworks for electric motor drives motivates their use in observer design under varying operating conditions [30]. Separately, online parameter estimation is addressed via modified flux SMO with simultaneous R_s and L_s estimation [31], ANN-based online estimation of rotor resistances and R_s in sensorless IM drives [32], and parameter estimation embedded into sensorless FOC for multiphase open-end winding IM [33].

Unsolved tasks become evident across these streams. Despite these extensive efforts, several open problems remain. A large portion of sensorless control studies focuses on speed or flux estimation while assuming a fixed R_s or compensating it only indirectly. Conversely, works dedicated to resistance estimation often lack a unified sensorless architecture that coherently integrates speed estimation and R_s adaptation within a IM FOC framework. Moreover, MRAS-based techniques may suffer from stability limitations and parameter sensitivity in low-speed regions, whereas SMO-based schemes require careful design to suppress chattering without sacrificing estimation accuracy. These limitations indicate the need for a sensorless control structure that simultaneously enhances low-speed robustness, preserves estimator stability, and explicitly accounts for R_s variations.

The goal of the paper is to develop an improved speed-sensorless control scheme for IM drives that maintains high accuracy of estimation under variations in R_s. The proposed approach improves robustness in low-speed operation and under thermal parameter drift while preserving dynamic performance and system stability.

Dynamic model of the IM. The electrical dynamics of the IM are described in the stationary (α, β) frame. Starting from the stator and rotor current equations, the derivatives of the stator current components can be rearranged as (1)–(4):

$$\frac{\mathrm{d}i_{s\alpha}}{\mathrm{d}t} = A\left(\frac{u_{s\alpha}}{L_m} - \frac{R_s}{L_m}i_{s\alpha} + \frac{R_r}{L_r}i_{r\alpha}\right) + A\left(\omega_r \frac{L_m}{L_r} i_{s\beta} + \omega_r i_{r\beta}\right); \quad (1)$$

$$\frac{\mathrm{d}i_{s\beta}}{\mathrm{d}t} = A\left(\frac{u_{s\beta}}{L_m} - \frac{R_s}{L_m}i_{s\beta} + \frac{R_r}{L_r}i_{r\beta}\right) - A\left(\omega_r \frac{L_m}{L_r} i_{s\alpha} + \omega_r i_{r\alpha}\right); \quad (2)$$

$$\frac{\mathrm{d}i_{r\alpha}}{\mathrm{d}t} = B\left(\frac{u_{s\alpha}}{L_s} - \frac{R_s}{L_s}i_{s\alpha} + \frac{R_r}{L_m}i_{r\alpha}\right) + B\left(\omega_r \frac{L_r}{L_m} i_{r\beta} + \omega_r i_{s\beta}\right); \quad (3)$$

$$\frac{\mathrm{d}i_{r\beta}}{\mathrm{d}t} = B\left(\frac{u_{s\beta}}{L_s} - \frac{R_s}{L_s}i_{s\beta} + \frac{R_r}{L_m}i_{r\beta}\right) - B\left(\omega_r \frac{L_r}{L_m} i_{r\alpha} + \omega_r i_{s\alpha}\right), \quad (4)$$

where $i_{s\alpha}$, $u_{s\alpha}$ are the stator current and voltage along the stationary α-axis; $i_{s\beta}$, $u_{s\beta}$ are the stator current and voltage along the stationary β-axis; R_s, R_r are the stator and rotor resistances; L_s, L_r, L_m are the stator, rotor and magnetizing inductances; ω_m is the mechanical speed; $\omega_r = p\omega_m$ is the rotor electrical speed; p is the number of pole pairs.

In these expressions, the coefficients A and B are:

$$A = L_m L_r / (L_s L_r - L_m^2); \quad B = L_s L_m / (L_m^2 - L_s L_r).$$

The relationship between the electromagnetic torque and the load torque is:

$$\frac{\mathrm{d}\omega_r}{\mathrm{d}t} = \frac{p}{J}\left(T_e - T_L\right), \quad (5)$$

where J is the inertia; T_e, T_L are the electromagnetic and load torque, respectively.

Speed estimation based on SMO. SMO estimates rotor speed from measured stator currents and voltages. Using the IM model in the stationary reference frame, it reconstructs stator current and rotor flux dynamics from these signals, as defined in equations (6)–(9):

$$\begin{cases} \dfrac{\mathrm{d}i_{s\alpha,est}}{\mathrm{d}t} = c_1 i_{s\alpha,est} + c_2\left(\dfrac{1}{T_r}\psi_{r\alpha,est}^{SMO} + \omega_{r,est}\psi_{r\beta,est}^{SMO}\right) + \\ + \dfrac{1}{\sigma L_s}u_{s\alpha} + \left(-d_{11}sat\left(e_{i\alpha}\right) + d_{12}sat\left(e_{i\beta}\right)\right); \end{cases} \quad (6)$$

$$\begin{cases} \dfrac{\mathrm{d}i_{s\beta,est}}{\mathrm{d}t} = c_1 i_{s\beta,est} + c_2\left(\dfrac{1}{T_r}\psi_{r\beta,est}^{SMO} - \omega_{r,est}\psi_{r\alpha,est}^{SMO}\right) + \\ + \dfrac{1}{\sigma L_s}u_{s\beta} - \left(d_{11}sat\left(e_{i\beta}\right) + d_{12}sat\left(e_{i\alpha}\right)\right); \end{cases} \quad (7)$$

$$\begin{cases} \dfrac{\mathrm{d}\psi_{r\alpha,est}^{SMO}}{\mathrm{d}t} = \dfrac{L_m}{T_r} i_{s\alpha,est} - \dfrac{1}{T_r}\psi_{r\alpha,est}^{SMO} - \\ -\omega_{r,est}\psi_{r\beta,est}^{SMO} + \left(-d_{21} sat\left(e_{i\alpha}\right) + d_{22} sat\left(e_{i\beta}\right)\right), \end{cases} \quad (8)$$

$$\begin{cases} \dfrac{\mathrm{d}\psi_{r\beta,est}^{SMO}}{\mathrm{d}t} = \dfrac{L_m}{T_r} i_{s\beta,est} - \dfrac{1}{T_r}\psi_{r\beta,est}^{SMO} + \\ +\omega_{r,est}\psi_{r\alpha,est}^{SMO} - \left(d_{21} sat\left(e_{i\beta}\right) + d_{22} sat\left(e_{i\alpha}\right)\right), \end{cases} \quad (9)$$

where:

$$c_1 = -\frac{R_{s,est} + \left(\dfrac{L_m}{L_r}\right)^2 R_r}{\sigma L_s};\ c_2 = \frac{L_m}{\sigma L_s L_r};$$

$$\sigma = \left(1 - \frac{L_m^2}{L_s L_r}\right);\quad T_r = L_r / R_r;\quad \lambda = 1/(L_s L_r - L_m^2);$$

$$e_{i\alpha} = i_{s\alpha,m} - i_{s\alpha,est};\quad e_{i\beta} = i_{s\beta,m} - i_{s\beta,est};$$
$$d_{11} = -\lambda(C-1)(R_{s,est}L_r + R_r L_s);\quad d_{12} = (C-1)\omega_{r,est};$$
$$d_{21} = (C-1)(R_r L_s - C R_{s,est} L_r)/L_m;$$
$$d_{22} = -(C-1)\omega_{r,est}/(\lambda L_m);\quad C > 1;$$

where $i_{s\alpha,m}$, $i_{s\beta,m}$ are the measured stator currents; $i_{s\alpha,est}$, $i_{s\beta,est}$ are their estimated values; $\psi_{r\alpha,est}^{SMO}$, $\psi_{r\beta,est}^{SMO}$ are the rotor flux components estimated from the SMO. By properly selecting the observer gains, the sliding conditions $e_{i\alpha}\to 0$ and $e_{i\beta}\to 0$ are enforced in finite time, ensuring robust convergence of the current estimates despite parameter uncertainties.

In these equations, the discontinuous correction terms are governed by a saturation function, defined as:

$$\mathrm{sat}(x) = \max[-1, \min(1, x/\Delta)], \quad (10)$$

where Δ is the positive constant.

Once the sliding regime is established, the rotor speed is extracted through a scalar deviation signal constructed from the stator current estimation error and the estimated rotor flux components:

$$\varepsilon_\omega = \left(i_{s\alpha,m} - i_{s\alpha,est}\right)\psi_{r\beta,est}^{SMO} - \left(i_{s\beta,m} - i_{s\beta,est}\right)\psi_{r\alpha,est}^{SMO}. \quad (11)$$

This signal reflects the mismatch between the estimated electromagnetic state and the actual motor behavior and serves as a physically meaningful indicator of speed adaptation.

The estimated rotor electrical speed is then obtained via a PI adaptation mechanism:

$$\omega_{r,est} = K_{p,\omega}\varepsilon_\omega(t) + K_{i,\omega}\int_0^T \varepsilon_\omega(t)\mathrm{d}t, \quad (12)$$

where $K_{p,\omega}$, $K_{i,\omega}$ are the proportional and integral gains of the PI controller used in the speed estimation loop.

The proposed SMO relies only on measured stator voltages and currents and provides robust speed estimation, which naturally motivates the incorporation of a R_s estimation scheme in the next section.

***R_s* estimation based on the SMO-MRAS structure.** A rotor-flux MRAS-based resistance adaptation mechanism is proposed to compensate R_s variations. The rotor flux from the voltage model is the reference, and the observer-based flux is the adaptive model; their difference is used to estimate the R_s. The complete SMO-MRAS scheme for joint speed and R_s estimation is shown in Fig. 1.

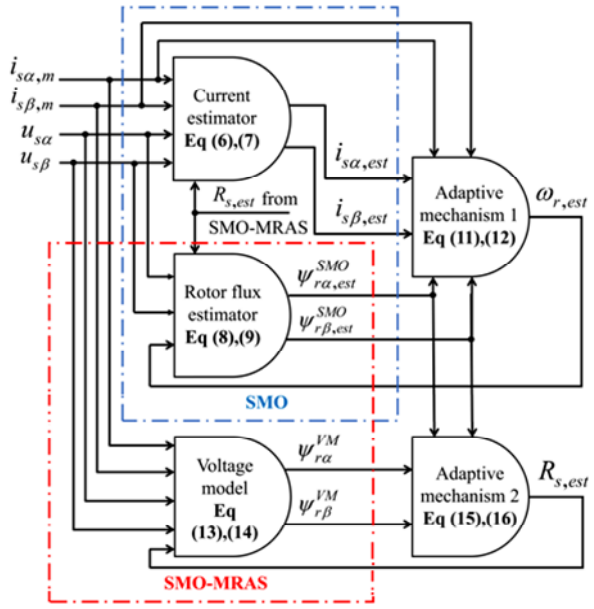

Fig. 1. Block diagram of the SMO scheme for speed estimation and the SMO-MRAS scheme for R_s estimation

In practical IM drives, the R_s varies with temperature due to thermal effects, and this variation becomes significant during low-speed operation and thermal transients. It has been reported that neglecting such resistance changes leads to inaccurate flux estimation and degraded drive performance, underscoring the need for stator estimation [34–36].

To address this issue, a R_s estimation scheme is developed by integrating the proposed SMO-MRAS. In the proposed structure, the voltage model is selected as the reference model, since it explicitly reflects the influence of R_s as:

$$\frac{\mathrm{d}\psi_{r\alpha}^{VM}}{\mathrm{d}t} = \gamma\left(u_{s\alpha} - R_{s,est} i_{s\alpha,m}\right) - \gamma\delta\frac{\mathrm{d}i_{s\alpha}}{\mathrm{d}t}; \quad (13)$$

$$\frac{\mathrm{d}\psi_{r\beta}^{VM}}{\mathrm{d}t} = \gamma\left(u_{s\beta} - R_{s,est} i_{s\beta,m}\right) - \gamma\delta\frac{\mathrm{d}i_{s\beta}}{\mathrm{d}t}; \quad (14)$$

where the coefficients $\gamma = L_r / L_m$ and $\delta = (L_s L_r - L_m^2)/L_r$; $\psi_{r\alpha}^{VM}$, $\psi_{r\beta}^{VM}$ are the rotor flux components calculated from the voltage model.

The adaptive model employs the rotor flux estimated by the SMO, which exhibits reduced sensitivity to parameter uncertainties. The mismatch between the reference and adaptive flux estimates is used to form an adaptation deviation, which is processed by a PI mechanism to obtain the estimated R_s:

$$\varepsilon_{R_s} = \left(\psi_{r\alpha}^{SMO} - \psi_{r\alpha}^{VM}\right)\cdot i_{s\alpha,m} + \left(\psi_{r\beta}^{SMO} - \psi_{r\beta}^{VM}\right)\cdot i_{s\beta,m}; \quad (15)$$

$$R_{s\_est} = K_{p,R_s}\varepsilon_{R_s}(t) + K_{i,R_s}\int_0^T \varepsilon_{R_s}(t)\mathrm{d}t; \quad (16)$$

where K_{p,R_s}, K_{i,R_s} are the proportional and integral gains of the PI controller used in the R_s estimation loop.

The completed control architecture of the proposed speed-sensorless FOC drive integrating the SMO and SMO-MRAS mechanisms is illustrated in Fig. 2.

As shown in Fig. 2, the SMO provides the estimated rotor speed information required by the FOC scheme, while the SMO-MRAS loop operates in parallel to adapt the R_s. The two estimation mechanisms are structurally decoupled but dynamically coupled via electrical measurements, thereby enhancing robustness against parameter variations.

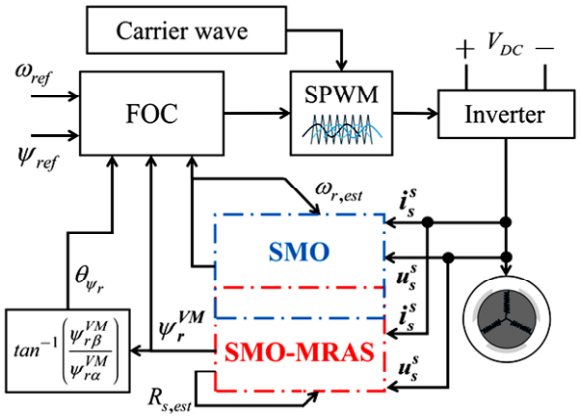

Fig. 2. Control structure of the proposed speed sensorless FOC with SMO and SMO-MRAS mechanisms

To quantitatively evaluate the control performance, the following indices are adopted (17) – (20):

- integral absolute error (IAE) is:

$$IAE = \int_0^T \left|\omega_{ref}(t) - \omega_{m,est}(t)\right| dt ; \quad (17)$$

- integral squared error (ISE) is:

$$ISE = \int_0^T \left(\omega_{ref}(t) - \omega_{m,est}(t)\right)^2 dt ; \quad (18)$$

- integral time squared error (ITSE) is:

$$ITSE = \int_0^T t\left(\omega_{ref}(t) - \omega_{m,est}(t)\right)^2 dt ; \quad (19)$$

where ω_{ref} is the reference speed; $\omega_{m,est}$ is the mechanical estimated speed.

Maximum stator current deviation:

$$\xi_{I,\max} = \max_{t\in[0,T]} \left\| i_{s,m}(t)\right| - \left|i_{s,est}(t)\right\| ; \quad (20)$$

where $\left|i_{s,m}\right| = \sqrt{i_{s\alpha,m}^2 + i_{s\beta,m}^2}$; $\left|i_{s,est}\right| = \sqrt{i_{s\alpha,est}^2 + i_{s\beta,est}^2}$.

Simulation. The drive system is simulated using the FOC method with the following IM parameters (Table 1).

Table 1

Parameters of a IM [25]

Parameter	Value
Power P, W	2200
Rated frequency f, Hz	50
Stator/rotor resistance R_s / R_r, Ω	3.179/2.118
Stator/rotor inductance L_s / L_r, H	0.209/0.209
Magnetizing inductance L_m, H	0.192

Simulation case 1 – without SMO-MRAS R_s estimation. Figures 3–5 illustrates the dynamic behavior of the sensorless FOC drive based on the SMO when the R_s variation is not compensated. During the acceleration phase from 0 to 0.5 s, the motor speed accurately follows the reference and remains stable at 20 rad/s under nominal parameter conditions. However, when the actual R_s increases by 20 % at t = 1 s (Fig. 3), the mismatch between the real motor parameters and the fixed resistance value used in the observer leads to a degradation in rotor flux estimation.

This parameter mismatch directly affects the SMO-based speed estimation mechanism. As observed in Fig. 4, the estimated rotor speed begins to exhibit noticeable oscillations after t = 1 s, which subsequently propagate to the actual motor speed through the FOC loop. The situation becomes more severe when the R_s increases by an additional 40 % at t = 2.5 s, resulting in amplified speed oscillations and reduced stability margins, particularly under the increasing load torque applied at t = 2 s.

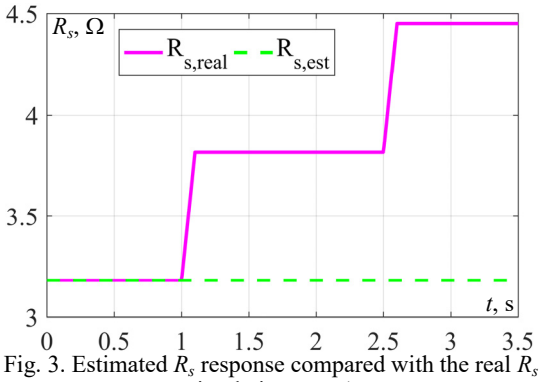

Fig. 3. Estimated R_s response compared with the real R_s simulation case 1

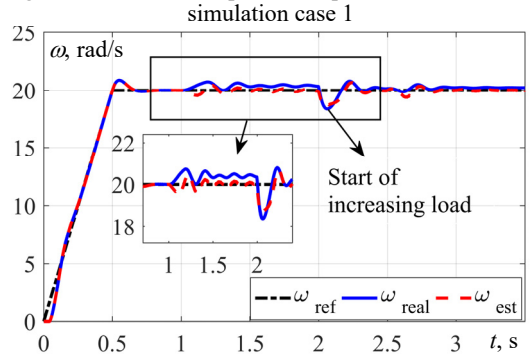

Fig. 4. Response speed in simulation case 1

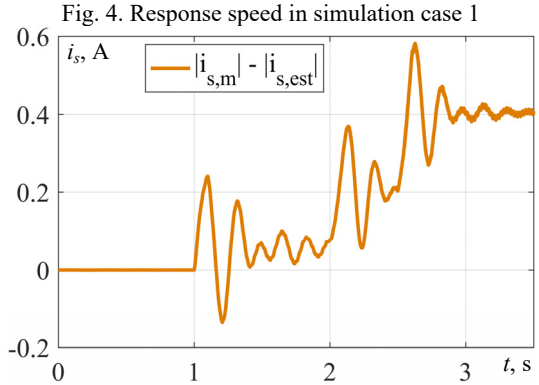

Fig. 5. Stator current magnitude deviation between measured and estimated values in simulation case 1

The underlying cause of this behavior is clarified in Fig. 5, which shows the deviation between the measured stator current magnitude and its estimated counterpart. As the R_s deviates from its nominal value, the current estimation deviation increases significantly, indicating that the SMO can no longer accurately reconstruct the stator current dynamics. Since the SMO relies on these estimated currents to generate the speed adaptation signal, the growing current mismatch leads to erroneous speed estimation and deteriorated closed-loop performance.

Simulation case 2 – with SMO-MRAS R_s estimation. Figures 6–8 present the dynamic performance of the proposed speed-sensorless FOC scheme when the SMO-MRAS-based R_s estimation is enabled. Under nominal conditions (0–1 s), the motor accelerates to the reference speed of 20 rad/s and maintains steady-state operation without noticeable oscillations, similar to Case 1. However, the system response differs significantly once the R_s varies.

As shown in Fig. 7, when the actual R_s increases by 20 % at t = 1 s and by 40 % at t = 2.5 s, the estimated resistance $R_{s,est}$ rapidly converges to the new real values with minimal transient deviation. The adaptation mechanism operates smoothly, without inducing oscillatory behavior, indicating that the SMO-MRAS structure effectively tracks parameter variations caused by thermal effects. The impact of accurate

resistance estimation is clearly reflected in the current reconstruction performance. Figure 8 shows that the deviation between the measured and estimated stator current magnitudes remains close to zero even after the resistance changes. Unlike Case 1, the current estimation error does not grow with increasing parameter mismatch, confirming that the observer model remains dynamically consistent with the actual motor behavior. Consequently, the speed response in Fig. 6 remains stable and well-regulated throughout the entire simulation.

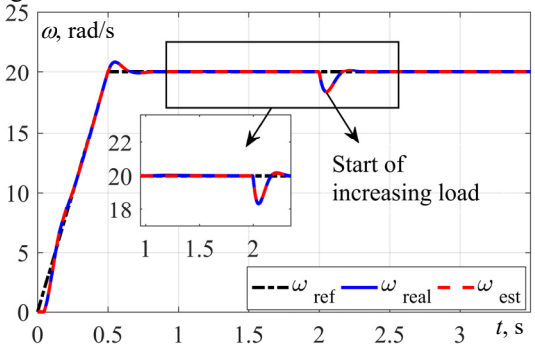

Fig. 6. Response speed in simulation case 2

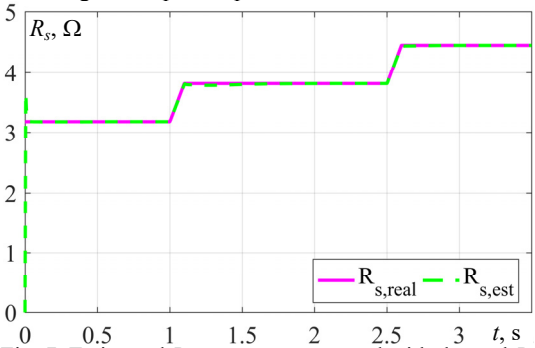

Fig. 7. Estimated R_s response compared with the real R_s simulation case 2

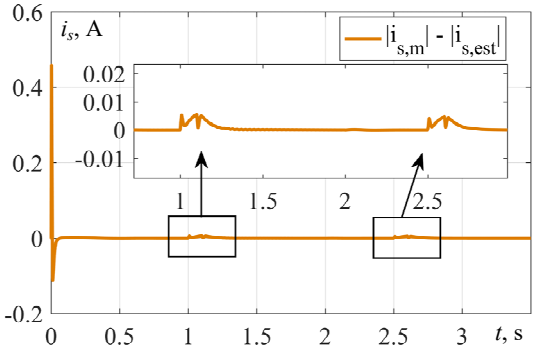

Fig. 8. Stator current magnitude deviation between measured and estimated values in simulation case 2

Although a temporary speed dip occurs at $t = 2$ s due to the increased applied load, both the real and estimated speeds rapidly recover to the reference value without sustained oscillations. Importantly, no instability or amplified ripple is observed after the 20 % and 40 % resistance increments, demonstrating that the SMO-based speed estimation is no longer degraded by parameter drift.

Discussion. Figure 9 quantitatively confirms the superiority of the proposed SMO-MRAS scheme.

In simulation Case 1 (without R_s estimation), the performance indices are *IAE*=0.7699, *ISE*=0.555, *ITSE*=0.6286, with a maximum current deviation of 0.578 A. When the SMO-MRAS mechanism is activated (Case 2), these values are reduced to *IAE*=0.4661, *ISE*=0.4688, *ITSE*=0.4502, and a maximum current deviation of 5.457 mA.

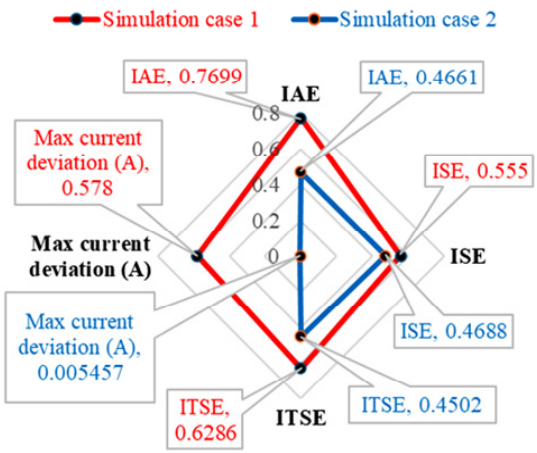

Fig. 9. Performance index comparison of the proposed scheme with and without SMO-MRAS resistance estimation

These results show that although the SMO provides robust speed estimation, it is sensitive to parameter mismatch. Integrating SMO-MRAS compensates for stator resistance variation, preserving current estimation accuracy and improving overall stability.

Moreover, under simultaneous load disturbance and 20–40 % R_s variations, the conventional scheme exhibits larger current estimation errors and speed oscillations, whereas the proposed approach maintains accurate current reconstruction and stable speed tracking, confirming its robustness under practical conditions.

Conclusions. This paper developed a robust speed-sensorless control scheme for IM drives under R_s variation. The proposed SMO-MRAS framework maintains accurate current reconstruction and stable speed estimation despite large parameter changes.

Simulations show that integrating R_s estimation significantly improves performance and robustness over conventional SMO-based methods, indicating strong potential for sensorless IM drives under thermal and load disturbances.

In the future, it is necessary to conduct experimental studies of effectiveness of improvement of robustness against thermal parameter variation and improves the reliability of sensorless IM drives in real operating conditions based on proposed method.

Acknowledgment. This research is funded by Ton Duc Thang University.

Conflict of interest. The authors declare that they have no conflicts of interest.

REFERENCES

1. Rezgui S.E., Darsouni Z., Benalla H. Nonlinear vector control of multiphase induction motor using linear quadratic regulator and active disturbances rejection control under disturbances and parameter variations. *Electrical Engineering & Electromechanics*, 2025, no. 6, pp. 75-83. doi: https://doi.org/10.20998/2074-272X.2025.6.10.

2. Giraldo E. Adaptive indirect field oriented linear control of an induction motor. *IAENG International Journal of Applied Mathematics*, 2022, vol. 52, no. 1, pp. 18-23. Available at: https://www.iaeng.org/IJAM/issues_v52/issue_1/IJAM_52_1_03.pdf.

3. Zellouma D., Bekakra Y., Benbouhenni H. Field-oriented control based on parallel proportional–integral controllers of induction motor drive. *Energy Reports*, 2023, vol. 9, pp. 4846-4860. doi: https://doi.org/10.1016/j.egyr.2023.04.008.

4. Mehedi I.M., Saad N., Magzoub M.A., Al-Saggaf U.M., Milyani A.H. Simulation Analysis and Experimental Evaluation of Improved Field-Oriented Controlled Induction Motors Incorporating Intelligent Controllers. *IEEE Access*, 2022, vol. 10, pp. 18380-18394. doi: https://doi.org/10.1109/ACCESS.2022.3150360.

5. Alnaib I.I., Alsammak A.N. Optimization of fractional PI controller parameters for enhanced induction motor speed control via indirect field-oriented control. *Electrical Engineering & Electromechanics*, 2025, no. 1, pp. 3-7. doi: https://doi.org/10.20998/2074-272X.2025.1.01.

6. Bach D.H., Tran C.D. An improved voltage model based on stator resistance estimation for FOC technique in the induction motor drive. *Advances in Electrical and Electronic Engineering*, 2024, vol. 22, no. 2, pp. 107-114. doi: https://doi.org/10.15598/aeee.v22i2.5745.
7. Wu X., Huang W., Lin X., Jiang W., Zhao Y., Zhu S. Direct Torque Control for Induction Motors Based on Minimum Voltage Vector Error. *IEEE Transactions on Industrial Electronics*, 2021, vol. 68, no. 5, pp. 3794-3804. doi: https://doi.org/10.1109/TIE.2020.2987283.
8. Mahfoud S., Derouich A., Ouanjli N.El, Mahfoud M.El. Enhancement of the Direct Torque Control by using Artificial Neuron Network for a Doubly Fed Induction Motor. *Intelligent Systems with Applications*, 2022, vol. 13, art. no. 200060. doi: https://doi.org/10.1016/j.iswa.2022.200060.
9. Guedida S., Tabbache B., Nounou K., Idir A. Reduced-Order Fractionalized Controller for Disturbance Compensation Based on Direct Torque Control of DSIM With Less Harmonic. *Electrica*, 2024, vol. 24, no. 2, pp. 450-462. doi: https://doi.org/10.5152/electrica.2024.23194.
10. Moussaoui L. Performance enhancement of direct torque control induction motor drive using space vector modulation strategy. *Electrical Engineering & Electromechanics*, 2022, no. 1, pp. 29-37. doi: https://doi.org/10.20998/2074-272X.2022.1.04.
11. Travieso-Torres J.C., Duarte-Mermoud M.A., Díaz M., Contreras-Jara C., Hernández F. Closed-Loop Adaptive High-Starting Torque Scalar Control Scheme for Induction Motor Variable Speed Drives. *Energies*, 2022, vol. 15, no. 10, art. no. 3489. doi: https://doi.org/10.3390/en15103489.
12. Travieso-Torres J.C., Contreras-Jara C., Diaz M., Aguila-Camacho N., Duarte-Mermoud M.A. New Adaptive Starting Scalar Control Scheme for Induction Motor Variable Speed Drives. *IEEE Transactions on Energy Conversion*, 2022, vol. 37, no. 1, pp. 729-736. doi: https://doi.org/10.1109/TEC.2021.3108664.
13. Tran C.D., Kuchar M., Sotola V., Nguyen P.D. Sensor fault diagnosis strategy based on rotor flux observers in three-phase induction motor drive. *Scientific Reports*, 2025, vol. 16, no. 1, art. no. 267. doi: https://doi.org/10.1038/s41598-025-29381-9.
14. Szoke E., Szabo C., Pintilie L.-N. Artificial Intelligence-Based Sensorless Control of Induction Motors with Dual-Field Orientation. *Applied Sciences*, 2025, vol. 15, no. 16, art. no. 8919. doi: https://doi.org/10.3390/app15168919.
15. Tan L.N., Cong T.P., Cong D.P. Neural Network Observers and Sensorless Robust Optimal Control for Partially Unknown PMSM With Disturbances and Saturating Voltages. *IEEE Transactions on Power Electronics*, 2021, vol. 36, no. 10, pp. 12045-12056. doi: https://doi.org/10.1109/TPEL.2021.3071465.
16. Gamazo-Real J.-C., Martínez-Martínez V., Gomez-Gil J. ANN-based position and speed sensorless estimation for BLDC motors. *Measurement*, 2022, vol. 188, art. no. 110602. doi: https://doi.org/10.1016/j.measurement.2021.110602.
17. Alnaib I.I., Alsammak A.N., Mohammed K.K. Brushless DC motor drive with optimal fractional-order sliding-mode control based on a genetic algorithm. *Electrical Engineering & Electromechanics*, 2025, no. 2, pp. 19-23. doi: https://doi.org/10.20998/2074-272X.2025.2.03.
18. Chebaani M., Mahmoud M.M., Tazay A.F., Mosaad M.I., Nouraldin N.A. Extended Kalman Filter design for sensorless sliding mode predictive control of induction motors without weighting factor: An experimental investigation. *PLOS ONE*, 2023, vol. 18, no. 11, art. no. e0293278. doi: https://doi.org/10.1371/journal.pone.0293278.
19. Di Girolamo S., Sferlazza A., Pipitone E., Caltabellotta S., Cirrincione M. Sensorless control of permanent magnet synchronous motor for exhaust energy recovery of internal combustion engine: a comparison between Kalman filter and MRAS observer. *Systems Science & Control Engineering*, 2024, vol. 12, no. 1, art. no. 2322067. doi: https://doi.org/10.1080/21642583.2024.2322067.
20. Janiszewski D. Sensorless Model Predictive Control of Permanent Magnet Synchronous Motors Using an Unscented Kalman Filter. *Energies*, 2024, vol. 17, no. 10, art. no. 2387. https://doi.org/10.3390/en17102387.
21. Korzonek M., Tarchala G., Orlowska-Kowalska T. Simple Stability Enhancement Method for Stator Current Error-Based MRAS-Type Speed Estimator for Induction Motor. *IEEE Transactions on Industrial Electronics*, 2020, vol. 67, no. 7, pp. 5854-5866. doi: https://doi.org/10.1109/TIE.2019.2960726.
22. Zaky M.S., Metwaly M.K. Sensitivity Analysis of a Stator Current-based MRAS Estimator for Sensorless Induction Motor Drives. *Engineering, Technology & Applied Science Research*, 2024, vol. 14, no. 6, pp. 17584-17590. doi: https://doi.org/10.48084/etasr.8737.
23. Kubatko M., Bielesz D., Kirschner S., Hamani K., Kuchar M., Mrovec T., Prazenica M. Sensorless Direct Field-Oriented Control of Induction Motor Drive Using Artificial Neural Network-Based Reactive Power MRAS. *Sensors*, 2025, vol. 25, no. 23, art. no. 7135. doi: https://doi.org/10.3390/s25237135.
24. El Daoudi S., Lazrak L., El Ouanjli N., Ait Lafkih M. Sensorless fuzzy direct torque control of induction motor with sliding mode speed controller. *Computers and Electrical Engineering*, 2021, vol. 96, art. no. 107490. doi: https://doi.org/10.1016/j.compeleceng.2021.107490.
25. Tran C.D., Kuchar M., Nguyen P.D. Improved speed sensorless control for induction motor drives using rotor flux angle estimation. *Electrical Engineering & Electromechanics*, 2025, no. 6, pp. 93-97. doi: https://doi.org/10.20998/2074-272X.2025.6.12.
26. Rind S.J., Amjad A., Jamil M. Rotor Flux MRAS based Speed Sensorless Indirect Field Oriented Control of Induction Motor Drive for Electric and Hybrid Electric Vehicles. *2018 53rd International Universities Power Engineering Conference (UPEC)*, 2018, no. 1-6. doi: https://doi.org/10.1109/UPEC.2018.8542009.
27. Mao S., Tao H., Zheng Z. Sensorless Control of Induction Motors Based on Fractional-Order Linear Super-Twisting Sliding Mode Observer With Flux Linkage Compensation. *IEEE Access*, 2020, vol. 8, pp. 172308-172317. doi: https://doi.org/10.1109/ACCESS.2020.3024626.
28. Zhang L., Dong Z., Zhao L., Laghrouche S. Sliding Mode Observer for Speed Sensorless Linear Induction Motor Drives. *IEEE Access*, 2021, vol. 9, pp. 51202-51213. doi: https://doi.org/10.1109/ACCESS.2021.3067805.
29. Yang Z., Wang D., Sun X., Wu J. Speed sensorless control of a bearingless induction motor with combined neural network and fractional sliding mode. *Mechatronics*, 2022, vol. 82, art. no. 102721. doi: https://doi.org/10.1016/j.mechatronics.2021.102721.
30. Senani F., Rahab A., Benalla H. Performance evaluation and analysis by simulation for sliding mode control with speed regulation of permanent magnet synchronous motor drives in electric vehicles. *Electrical Engineering & Electromechanics*, 2025, no. 5, pp. 43-48. doi: https://doi.org/10.20998/2074-272X.2025.5.06.
31. Ye S., Yao X. A Modified Flux Sliding-Mode Observer for the Sensorless Control of PMSMs With Online Stator Resistance and Inductance Estimation. *IEEE Transactions on Power Electronics*, 2020, vol. 35, no. 8, pp. 8652-8662. doi: https://doi.org/10.1109/TPEL.2019.2963112.
32. Pham Van T., Vo Tien D., Leonowicz Z., Jasinski M., Sikorski T., Chakrabarti P. Online Rotor and Stator Resistance Estimation Based on Artificial Neural Network Applied in Sensorless Induction Motor Drive. *Energies*, 2020, vol. 13, no. 18, art. no. 4946. doi: https://doi.org/10.3390/en13184946.
33. Khadar S., Abu-Rub H., Kouzou A. Sensorless Field-Oriented Control for Open-End Winding Five-Phase Induction Motor With Parameters Estimation. *IEEE Open Journal of the Industrial Electronics Society*, 2021, vol. 2, pp. 266-279. doi: https://doi.org/10.1109/OJIES.2021.3072232.
34. Lazcano U., Poza J., Garramiola F., Rivera C.A., Iturbe I. Double Dead-Time Signal Injection Strategy for Stator Resistance Estimation of Induction Machines. *Applied Sciences*, 2022, vol. 12, no. 17, art. no. 8812. doi: https://doi.org/10.3390/app12178812.
35. Nguyen P.D., Kuchar M. Performance improvement of sensorless scalar and vector control for induction motor drives via an enhanced voltage model. *Electrical Engineering & Electromechanics*, 2026, no. 3, pp. 62-67. doi: https://doi.org/10.20998/2074-272X.2026.3.09.
36. Tran C.D., Kuchar M., Nguyen P.D. Improved rotor flux estimation for field-oriented control in induction motor drives. *Tekhnichna Elektrodynamika*, 2025, no. 6, pp. 52-57. doi: https://doi.org/10.15407/techned2025.06.052.

Received 25.01.2026
Accepted 26.04.2026
Published 02.07.2026

Q.T. Nguyen[1], *PhD Student,*
C.D. Tran[1], *Doctor on Electrical Engineering,*
[1] Power System Optimization Research Group,
Faculty of Electrical and Electronics Engineering,
Ton Duc Thang University, Ho Chi Minh City, Vietnam,
e-mail: trandinhcuong@tdtu.edu.vn (Corresponding Author)

How to cite this article:
Nguyen Q.T., Tran C.D. An enhanced sliding mode observer method applied to sensorless induction motor drives under stator resistance variation. *Electrical Engineering & Electromechanics*, 2026, no. 4, pp. 34-39. doi: https://doi.org/10.20998/2074-272X.2026.4.05